MATERIALS CHEMISTRY
FRONTIERS

CCS 中国化学会 CHINESE CHEMICAL SOCIETY
ICCAS
ROYAL SOCIETY OF CHEMISTRY

RESEARCH ARTICLE

View Article Online
View Journal | View Issue

Cite this: *Mater. Chem. Front.*, 2024, **8**, 2754

Sustainable food packaging using modified SiO_2 nanofillers in biodegradable polymers†

Mikhail Koreshkov, *[a] Sebastian J. Antreich, [a] Alexander Bismarck, [b] Ines Fritz, [c] Erik Reimhult, [a] Yuuki Takatsuna [a] and Ronald Zirbs *[a]

The need to switch to bio-based, biodegradable and/or fully recyclable polymers is becoming increasingly clear, especially in the area of food packaging, which is a major contributor to plastic pollution. To meet this challenge, biodegradable polymers must not only be economically viable, but also have properties that match or better those of conventional fossil-based polymers, such as robust mechanical strength and efficient gas barrier properties. One promising route is the production of composite materials from biodegradable polymers and SiO_2 nanoparticles. However, the high surface energy of SiO_2 often leads to agglomeration of the filler in the hydrophobic polymer matrix, which compromises the integrity of the composite. Here we present an innovative approach in which the surface of silica nanoparticles is modified with L-lactic acid oligomers (OLLA), effectively reducing the agglomeration of the filler and improving processability. Using conventional polymer processing methods that comply with industry standards, we prepared PLLA and PHBV nanocomposites and evaluated the effectiveness of the modification using a novel SBF-SEM technique. Our results show that modified silica achieves better dispersion in the polymer matrix and yields 70% more independent particles in the nanocomposite. The introduction of OLLA-*g*-SiO_2 increases the oxygen barrier of PLLA by 38% while accelerating the biodegradation rate and improving the toughness of the eco-friendly nanocomposites. This innovative approach offers a sustainable solution that is set to revolutionise the landscape of green food packaging.

Received 14th March 2024,
Accepted 13th June 2024

DOI: 10.1039/d4qm00206g

rsc.li/frontiers-materials

Introduction

For many years, there has been a concerted effort to promote sustainable lifestyles and the transition to a circular economy. This drive has had a profound impact on consumer behaviour and industrial practices. This includes areas where polymer materials are essential, such as food and beverage containers, packaging materials, recyclability, and ensuring the shelf life of products. The uncontrolled production of fossil-based polymers has already led to alarming levels of global pollution. Only 9% of all produced and used polymers are recycled, 12% are incinerated, and the remaining 79% accumulates in landfill sites or the natural environment.[1] Approximately half of the polymer waste is generated from single-use applications,[2] including food and beverage packaging.

Addressing these problems requires a comprehensive strategy involving legal regulation and policies, business innovation, and changes in consumer behavior. Many countries and organizations have already made significant progress in this direction, such as the ban on single-use plastics in the European Union and proposals for mandatory use of biodegradable polymers in product packaging.[3,4] The introduction of strict regulations was intended to focus primarily on the continuous improvement of recycling processes. However, problems such as contamination of packaging materials with food residues and odors highlight the economic difficulties of recycling affecting its profitability.[5] Therefore, the search for renewable alternatives to traditional fossil fuel-based polymers for food packaging remains a relevant research area.

Renewable polymers have received tremendous interest for food packaging.[6] Particularly notable are biodegradable polymers, such as polylactic acid (PLA), that can be degraded into harmless by-products under controlled composting conditions.[7] Polyhydroxyalkanoates (PHAs) are biodegradable when composted and in the soil or aquatic environments.[8] One well-known PHA is

[a] *Department of Bionanosciences, University of Natural Resources and Life Sciences (BOKU), Vienna, Austria. E-mail: mikhail.koreshkov@boku.ac.at, ronald.zirbs@boku.ac.at*
[b] *Polymer and Composite Engineering (PaCE) Group, Institute of Material Chemistry and Research, Faculty of Chemistry, University of Vienna, Vienna, Austria*
[c] *Department of Agrobiotechnology, Institute of Environmental Biotechnology, University of Natural Resources and Life Sciences (BOKU), IFA-Tulln, Tulln, Austria*

† Electronic supplementary information (ESI) available: SEM characterization of fractured films, stress–strain curves and SEM images of specimens after tensile tests, water absorption profiles, DSC measurements, scheme of general setup of the biodegradation tests. See DOI: https://doi.org/10.1039/d4qm00206g

poly(3-hydroxybutyrate-*co*-3-hydroxyvalerate) (PHBV). The properties of PHBV are determined by the co-monomer ratio.[9,10]

Despite the wide variety of biodegradable polymers, their use in food packaging faces serious challenges ranging from high production costs to insufficient mechanical strength, poor gas barrier properties, and limited processability using conventional polymer processing methods.[11] The industrial approach to developing competitive analogs of fossil-based polymers involves reinforcing biodegradable polymers with fillers to obtain environmentally friendly green composites that meet the stringent requirements of packaging materials.

The dispersion state of the filler within the polymer matrix plays a significant role in determining the properties of composite materials. To ensure homogeneous filler distribution, the industry often uses nanofillers.[12] The incorporation of various nanomaterials can significantly improve the properties of advanced polymer nanocomposites, which are crucial for the development of high-performance applications.[13–17] A well-known filler is nanosilica. SiO_2 is considered an environmentally friendly material and has attracted significant attention due to its abundance, low cost, transparency, large surface area, high hardness, and thermal stability.[18] Reducing the size of the SiO_2 nanoparticles increases the internal surface area that interacts with the polymer matrix, which is critical for the performance of the resulting polymer nanocomposites. However, silica nanoparticles have a high surface energy, which poorly matches the weaker molecular interactions of non-polar polymer matrices.[19] As a result, hydrophilic silica exhibits a natural incompatibility with hydrophobic polymers, such as PLA or PHBV, leading to the agglomeration of SiO_2 nanoparticles during compounding. The severe but rarely quantified agglomeration reduces the surface-to-volume ratio of the filler, which translates into poor mechanical toughness[20] and high gas permeability[21] of composite materials compared to its theoretical potential.

A promising approach to improve the distribution and enhancing the interaction between filler and renewable polymers is the chemical functionalization of the silica nanoparticles by grafting biodegradable polymers to their surfaces. Such core–shell nanoparticles emulate the physico-chemical properties of the polymer matrix and could tremendously improve dispersion. Combined with controlled polymerization reactions, the widely used "grafting from" synthetic strategy combines a high grafting density compared to "grafting to" methods enabling control over the molecular weight of the individual grafted chains.[22,23] A high surface density is essential to ensure uniform polymer shell properties. However, it is important to realize that a high polymer fraction, *i.e.*, high molecular weight chains, requires a higher filler fraction to provide the same silica nanoparticle loading.

The synthesis of core–shell SiO_2 nanoparticles requires multi-step synthesis schemes using solvents and unstable intermediates, making it economically unfeasible to scale.[24,25] Grafting polymer brushes onto silica mainly focused on chemical pretreatments of silica, often with toxic agents,[22,26] rendering such methods irrelevant for green composites. While literature is rife

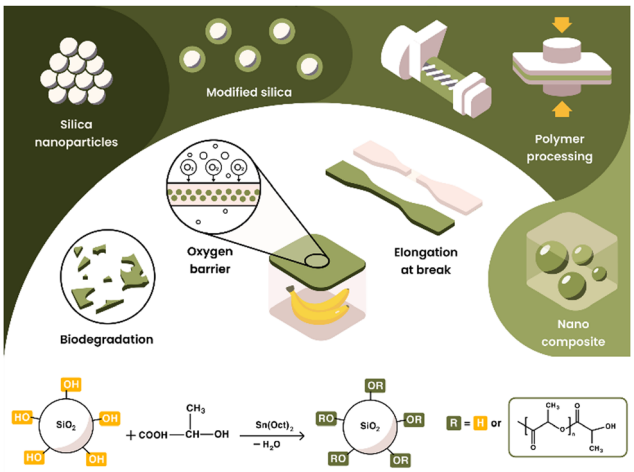

Fig. 1 Representation of the concept explored in this paper.

with examples of composites produced using conventional polymer processing methods,[24] the state of dispersion and distribution of (modified) silica fillers throughout the volume of the composites is rarely quantified; most works study the surface distribution of the filler, which may differ from the 3D bulk filler network.[27]

We demonstrate a straightforward and scalable solvent-free method to produce SiO_2 core–shell nanoparticles densely grafted with L-lactic acid oligomers (OLLA), which are innovative fillers for PLLA and PHBV (Fig. 1). Our approach is based on the use of economically feasible lactic acid as a compatibilizer between hydrophilic silica and hydrophobic polymer matrices in a one-step synthesis without utilization of unstable intermediates or chemical pretreatment of silica. The scalability of the process is further enhanced by the use of conventional polymer processing methods, such as extrusion, injection and compression molding for composites production. The comprehensive evaluation of composites shows that OLLA-grafted SiO_2 nanoparticles (OLLA-*g*-SiO_2) improve biodegradability, barrier and mechanical properties to meet the requirements for food packaging. Additionally, the state of dispersion and distribution of silica nanoparticles in biodegradable composites is characterized for the first time using serial block face SEM. This method represents a novel approach to visualize the 3D bulk filler network of nanocomposites and highlight the importance of surface modification for nanoscale dispersion of silica-based fillers within a polymer matrix.

Our results aim to demonstrate the potential of using bio-based and biodegradable polymers with well-dispersed SiO_2 nanoparticles to highlight the feasibility of green nanocomposites that offer a sustainable solution for food packaging.

Experimental

Materials

PLLA was purchased from Biomer (L9000, MW $\geq$ 150 kg mol^{-1}, D-content $\approx$ 1.5%) and PHBV from Tianan Biological Materials

(ENMAT Y1000P, HV content 8%, injection molding grade, with <0.5% boron nitride as nucleating agent and antioxidant Irganox 1010). 1,4-Dioxane and chloroform (Sigma-Aldrich, ≥99% purity) were used as solvents for PLLA and PHBV, respectively. Lactic acid (Aldrich, solute concentration: 85 wt%), sodium hydroxide (Aldrich, pellets, ≥98% purity), tin(II) 2-ethylhexanoate ($Sn(Oct)_2$, Aldrich, ≥85% purity), dichloromethane and alcohol were purchased from Sigma-Aldrich. Nano-SiO_2 (Aerosil, 200 ± 25 m^2 g^{-1}, ≥99% purity) was purchased from Roth.

Synthesis of OLLA-*g*-SiO_2

8 g of silica particles were dispersed in 300 mL water and mixed with aq. NaOH (35 g in 100 mL). After stirring for 20 s, 150 mL of lactic acid (LA) was added, and the resulting SiO_2-LA gel was precipitated and washed with LA. The resulting SiO_2-LA gel with additional 200 mL of LA was transferred to a three-neck flask equipped with a mechanical stirrer (Lab Mixer Overhead Stirrer PWR CV S1, IKA Werke, Germany) and a programmed temperature controller. The reaction mixture was stirred at 350 rpm and heated up to 100 °C using a heating mantle. After 2 h of continuous stirring at reduced pressure (20 mbar) to remove water, the temperature was increased to 110 °C and after a further 2 h to 120 °C for another 2 h. The catalyst $Sn(Oct)_2$ (1 wt% of monomer LA) was added to the system and stirred for 30 min under N_2. Then, the pressure was reduced to 20 mbar, and the polymerization carried initiated by a stepwise increase of the temperature to 130 °C for 2 h, 140 °C for 2 h, 150 °C for 2 h, and 160 °C for 4 h. After the reaction, the viscous mixture was poured into dichloromethane, centrifuged, and ethanol added. The precipitate was washed with dichloromethane four times and freeze-dried.

Processing of composites and the production of nanocomposite films

3 g of OLLA-*g*-SiO_2 was premixed with 57 g of PLLA and PHBV in 700 mL of dioxane and chloroform, respectively, which were subsequently vacuum dried. Prior to extrusion, both premixed composites were ground in a laboratory blender. The composites with OLLA-*g*-SiO_2 (5 wt%) were fed into a twin-screw micro-extruder (5 cm^3 micro-extruder, Xplore MC 5, Xplore Instruments B.V., Netherlands) and kept in the closed loop under N_2 environment at 180 °C and screw rotational speed of 100 rpm. After 2 min, the loop was opened, and the polymer melt was extruded at a screw rotation speed of 20 rpm. The extrudates were pelletized and compression molded into films with a thickness of ~470 μm using a hot press (Model 4126, Hydraulic Press, Carver, USA) at 180 °C applying a press force of 60 kN for 2 min. The resulting films were cooled in a room-temperature press under a force of 60 kN for 7 min. Dumbbell-shaped tensile specimens were produced using an injection molding system (HAAKE MiniJet, Thermo Scientific, Netherlands) and a mold (557-2298, ISO 527-2-5A) using a barrel temperature of 180 °C and a mold temperature of 45 °C.

Methods

Serial block face (SBF) SEM. SBF scans were performed on PLLA/OLLA-*g*-SiO_2 and PLLA/SiO_2 composites. The films were cut into cubes (around 1 × 1 × 1 mm) and glued with silver cement on a SEM stub. Glued blocks were trimmed with a glass knife on a UC-7 ultramicrotome (Leica Microsystems, Vienna, Austria) to 500 μm × 500 μm × 500 μm. They were coated with a 10 nm gold–palladium layer in an EM SCD005 sputter coater (Leica Microsystems) and mounted on the microtome of the Apreo SEM (Thermo Scientific, the Netherlands). Imaging was performed at 1.18 kV, 100 pA, 1 μs dwell time, and 4 times line integration. 45 slices with a slicing depth of 100 nm were made, controlled by the software Maps 3.4 VS (Thermo Fisher Scientific). The resulting stacks were aligned and registered in ImageJ with the plugin 'Linear stack alignment with SWIFT' using standard settings. The volume fraction of filler materials in the PLLA matrix and the number of particles were calculated, and 3D reconstruction of both composite materials was performed using ImageJ.

TEM. Transmission electron microscopy (TEM) images were recorded with an FEI Tecnai G2 (FEI Europe B.V., Austria) with 160 kV acceleration voltage. SiO_2 and OLLA-*g*-SiO_2 samples were dispersed in Milli-Q water and chloroform, respectively, sonicated for 10 min, and dried on carbon grids under ambient conditions.

NMR. ^{1}H NMR spectra were recorded at ambient temperature on a Bruker AV III 300 MHz spectrometer (Bruker Company, Switzerland) in dimethyl sulfoxide-d_6 (DMSO-d_6). The OLLA-*g*-SiO_2 (6 mg mL^{-1}) was dispersed in DMSO-d_6 and sonicated in an ultrasonic bath for 5 min.

Dynamic light scattering (DLS). DLS was performed to estimate the size distribution of filler material. The sample was dispersed in DMSO and sonicated for 10 min. DLS measurements were performed on a Malvern Zetasizer Nano-ZS dynamic light scattering device (Malvern Panalytical Ltd, Malvern, UK). The concentration of particles in DMSO was 1 mg mL^{-1}, and the measurements were performed at 25 °C.

Thermogravimetric analysis (TGA). TGA was performed on a Mettler Toledo TGA/DSC (Mettler Toledo GmbH, Vienna, Austria) (80 mL min^{-1} nitrogen) to characterize the thermal stability of OLLA-*g*-SiO_2. The measurement was carried out at 25 to 50 °C with a heating rate of 10 K min^{-1}.

FTIR. The molecular structure of filler material was confirmed by Fourier Transform Infrared Spectroscopy (FT-IR) using an FT-IR ATR spectrometer (Vertex 70, Bruker Austria GmbH, Vienna, Austria) with 32 scans in the wavelength range of 650–4000 cm^{-1}. Samples were directly mounted on the ATR unit and measured with the pressure stamp.

Mechanical test. Tensile tests followed the ASTM D636 guidelines using a universal dual-column testing frame (Series 5969, Instron Ltd, Norwood, UK). The strain was recorded using a video extensometer (IMT-CAMO018, camera: GigE PoE, IMETRUM, UK) tracking black dots, which were painted on "dog-bone" specimens using an opaque black permanent marker. The testing rate was 0.5 mm min^{-1}.

Oxygen transmission rate. The oxygen transmission rate (OTR) was measured in a gas permeability tester (VAC-VBS, Labthink Instruments Co. Ltd, China). The tested area was a circular shape with a diameter of 80 mm. Tests were performed at ambient conditions using a proportional mode with a 10%

pressure difference. Prior to testing, specimens were conditioned in the machine for 4 h under vacuum. The oxygen transmission rate was calculated according to standard GB/T1038-2000. At least five replicates were tested for each material.

Water vapor transmission rate. Water vapor transmission rate (WVTR) was recorded using a WVTR Tester W3/031 (Lab think Instruments Co., China) according to standard GB/T 1037-1988. The relative humidity (RH) was fixed at 100% in the wet chamber and 10% in the dry chamber, yielding a driving force of 90% RH. Films with an area of 33.18 cm^2 was analyzed at the atmospheric pressure and a temperature of 38 °C. WVTR was determined gravimetrically by weighing the dishes with films every 90 min for 10 cycles.

Biodegradation tests. All biodegradation tests were set up as aquatic aerobic biodegradation tests according to the OECD 301B (modified Sturm test). We used a mineral medium (potassium and sodium phosphates, ammonium chloride, calcium chloride, magnesium sulfate, and iron(III) chloride) in 500 mL glass bottles (Shott) equipped with the fitting gas washing unit. The test volume included 400 mL, 10 mL of mixed bacterial inoculum, and the test substance equivalent to *ca.* 0.3 to 0.6 g of carbon. The carbon content of the substances was determined by element analysis with the photo-oxidation principle. Inocula were extracted from organic waste compost (by suspending active compost in warm tap water and removing stones and swimming particles) for thermophilic test conditions.

Results and discussion

Chemical and structural characterization of L-lactic acid-grafted SiO_2

The preparation of OLLA-grafted SiO_2 was quantified using FTIR, NMR, and TGA by comparing OLLA-*g*-SiO_2 to SiO_2, OLLA, and PLLA. ATR-FTIR spectra of these compounds are presented in Fig. 2A. The IR spectrum of OLLA-*g*-SiO_2 showed the characteristic PLLA bands at 1750, 1450, and 1200 cm^{-1}, which were assigned to the C=O stretching, methyl asymmetric deformation, and symmetric C–O–C stretching of the ester modes, respectively.[28] The characteristic SiO_2 bands at 450, 800, and 1075 cm^{-1} were observed, corresponding to the rocking, bending, and stretching modes of Si–O–Si bonds, respectively.[29]

TGA curves for OLLA-*g*-SiO_2 (Fig. 2B) exhibited organic mass loss attributed to the oligomer grafted on the SiO_2 surface. The estimated OLLA mass fraction ($wt\%_{OLLA}$) is 20 ± 2.3 wt%, consistent with previous findings of polylactic acid grafting onto silica.[30] The decomposition temperature roughly coincides with literature values for OLLA.[31]

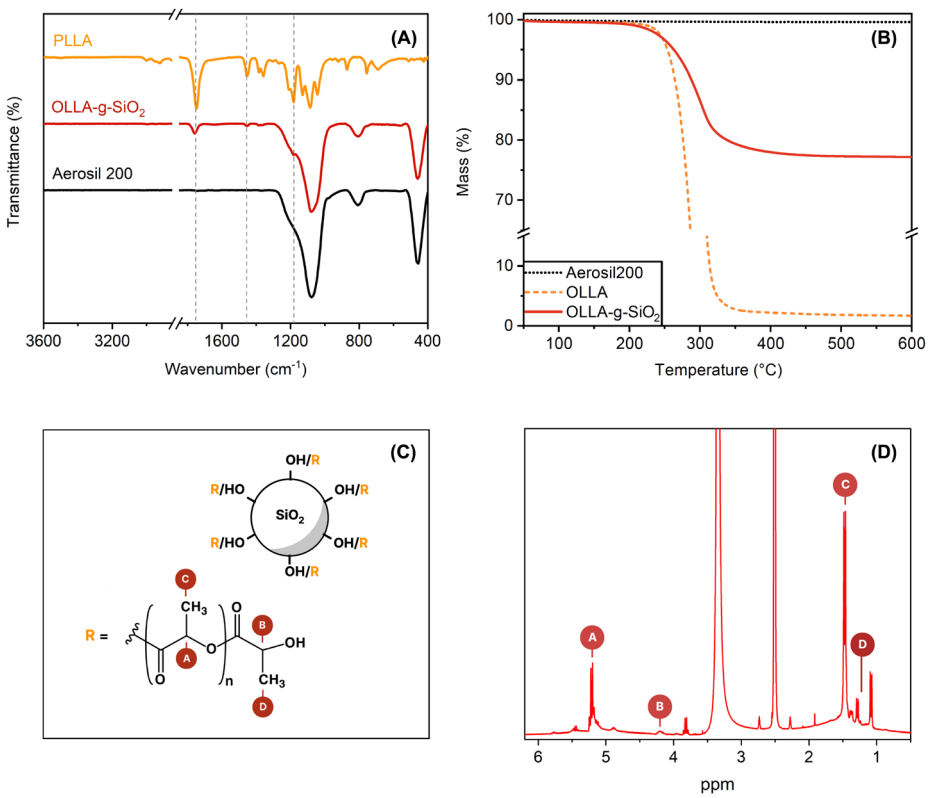

Fig. 2 Visual representation of analytical data depicting SiO_2, OLLA-*g*-SiO_2, and PLA; (A) FTIR spectra of OLLA-*g*-SiO_2, Aerosil 200, and PLLA show successful grafting of OLLA to SiO_2 nanoparticles. (B) Thermogravimetry data for SiO_2, OLLA, and OLLA-*g*-SiO_2. (C) Chemical structure of OLLA-*g*-SiO_2 marking the allocation of the NMR peaks in (D) ^{1}H-NMR spectra of OLLA-*g*-SiO_2.

OLLA grafted SiO_2 was further characterized by ^{1}H-NMR (Fig. 2D). By comparing the peak area of denoted peaks (Fig. 2C), we calculated the degree of polymerization of the grafted OLLA chains (DP_{OLLA}) using eqn (1) and the molar mass of the grafted molecules (MW_{OLLA}) using the molecular weight of 72 g mol^{-1} of lactyl (MW_{lactyl}) using eqn (2). The grafting density (σ_{OLLA}) was estimated using the specific surface of 200 m^2 g^{-1} for Aerosil 200 ($S_{Aerosil\ 200}$) and Avogadro's constant (N_A) using eqn (3).[22]

$$DP_{OLLA} = \frac{I_D + I_C}{I_D} \quad (1)$$

$$MW_{OLLA} = DP_{OLLA} \times MW_{lactyl} \quad (2)$$

$$\sigma_{OLLA} = \frac{wt\%_{OLLA} \times N_A}{(1 - wt\%_{OLLA}) \times MW_{OLLA} \times S_{Aerosil\ 200}} \quad (3)$$

The DP_{OLLA} was determined to be 6 ± 1.5, MW_{OLLA} was $4 \pm 1 \times 10^2$ (g mol^{-1}), and σ_{OLLA} was 1.9 ± 0.4 (chains per nm^2), indicating a ~260% higher grafting density of low molecular weight OLLA grafted to SiO_2 than was reported for SiO_2-*graft*-poly(L-lactide) synthesized by the "grafting from" method from LA.[22]

Size and morphology of (L-lactic acid-grafted) SiO_2

The size distribution of (OLLA-*g*-)SiO_2 particles and agglomerates was determined using dynamic light scattering (DLS) and transmission electron microscopy (TEM). Fig. 3A shows the number-weighted size distribution of OLLA-*g*-SiO_2 dispersions in DMSO, which was chosen as a dispersion medium because of its similar polarity to PLLA and PHBV. OLLA-*g*-SiO_2 dispersions are stable but seem to be formed by small nanoparticle aggregates. In contrast, SiO_2 aggregated in DMSO and the agglomerates precipitated. SiO_2 in DMSO consisted of clustered particles of 133 ± 37 nm in size and aggregates of 0.7 ± 0.2 μm in size. Aggregates larger than 300 nm comprised ~97% of the particle volume. The OLLA-*g*-SiO_2 clustered particles were predominantly nanoscale with 177 ± 48 nm in size, suggesting that OLLA polymerized on nanoscale clusters of SiO_2.

Agglomerates with diameters between 80 and 735 nm for OLLA-*g*-SiO_2 and between 368 nm and 823 nm for unmodified SiO_2 were observed by TEM (Fig. 3B and D). The observed agglomerate size correlated weakly with the dimensions and fractions quantified by DLS. SiO_2 exhibited clustering of agglomerates by drying of suspensions (Fig. 3C), unlike the modified SiO_2, which comprised individualized clusters.

Polymer/(OLLA-grafted) SiO_2 nanocomposites

We chose a filler loading of 5 wt% (core–shell) nanoparticles at or above the high end of filler concentrations typically used for high-performance silica nanocomposites produced by melt compounding.[32–34] Higher concentrations can easily lead to a decrease in performance, typically attributed to increased aggregation of the filler within the matrix.[35,36] We hypothesized that the core–shell nature will improve the interfacial compatibility between the nanofiller and polymer matrix, leading to improved dispersibility as indicated by DLS in DMSO. Homogeneous distribution of SiO_2 cores in the polymer matrix should enhance barrier and mechanical properties. Hence, we characterized the size and distribution of (OLLA-*g*-)SiO_2 in the nanocomposites.

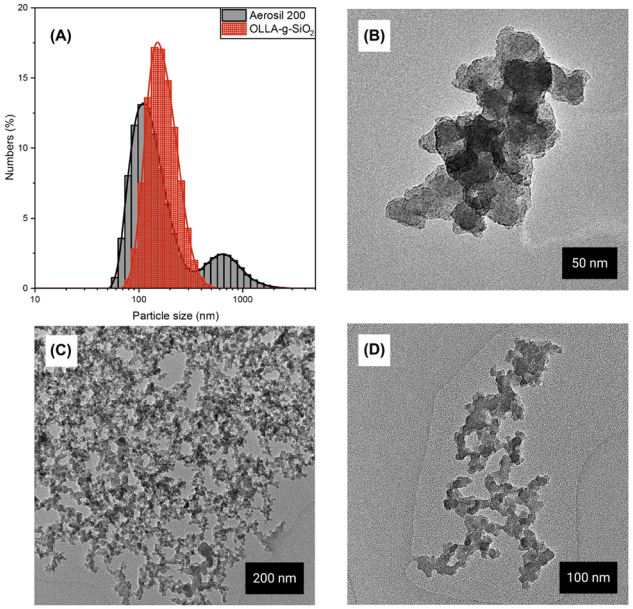

Fig. 3 DLS and TEM analytics of filler materials; (A) number-weighted size distributions measured by DLS for OLLA-*g*-SiO_2 and SiO_2 (Aerosil 200) in DMSO. (B) TEM micrographs of agglomerates of OLLA-*g*-SiO_2 nanoparticles, (C) clustered agglomerates of SiO_2 nanoparticles, and (D) agglomerates of SiO_2 nanoparticles.

State of dispersion of SiO_2 nanoparticles

The improved dispersibility of OLLA-*g*-SiO_2 nanoparticles compared to unmodified SiO_2 nanoparticles in PLLA or PHBV was evidenced by microscopic inspection of the film cross-sections using SEM (*cf.* Fig. 4A and D). Micrometer-sized aggregates are visible for nanocomposites containing unmodified SiO_2, while the OLLA-*g*-SiO_2 are dispersed at the nanoscale, in size roughly equal to those observed by DLS.

We used serial block-face scanning electron microscopy (SBF-SEM) to visualize the 3D dispersion of SiO_2 nanoparticles in PLLA nanocomposites. By this method, we sequentially remove slices of the composite *in situ* and image each exposed surface with SEM to reconstruct the 3D distribution of nanoscale objects. The commercially available PHBV Enmat Y1000P contains boron nitride and antioxidant additives that form nanoparticles. We could not distinguish additive nanoparticles from silica particles (Fig. S1D, ESI†). Therefore, our results are limited to PLLA nanocomposites, but we expect similar results for PHBV produced following the same protocol for unmodified *vs.* OLLA-grafted SiO_2 nanoparticles.

For both PLLA nanocomposites, the scanning electron micrographs revealed an imperfect filler dispersion in the PLLA matrix. OLLA-*g*-SiO_2 and unmodified SiO_2 are shown in Fig. 4B and E, respectively. In the 3D images, the colored areas represent SiO_2 particles (primary SiO_2 clusters and SiO_2 agglomerates).

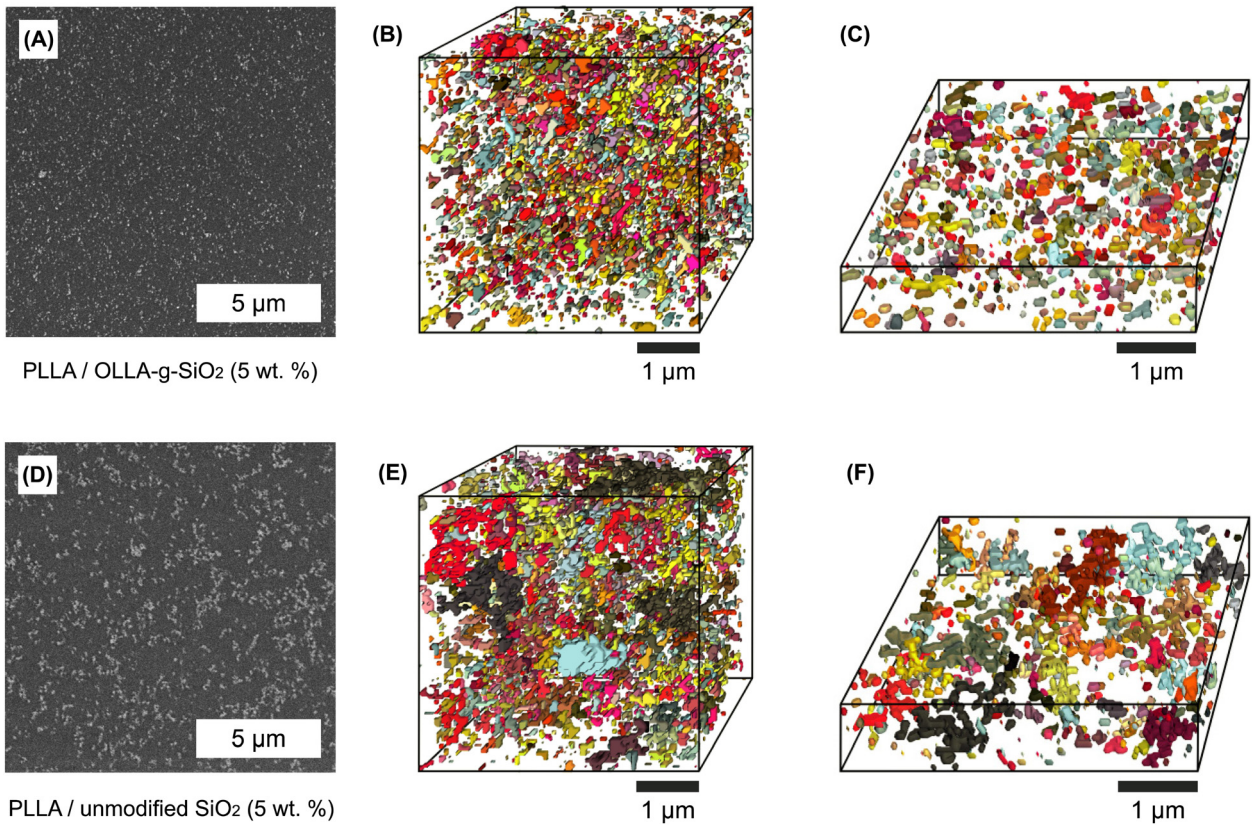

Fig. 4 Cross-sections of films produced by compression molding of (A) PLLA/OLLA-*g*-SiO_2 (5 wt%) and (D) PLLA/SiO_2 (5 wt%). 3D reconstructed SEM images of PLLA nanocomposites containing (B) OLLA-*g*-SiO_2 and (E) SiO_2 particles used for analysis. (C) and (F) Show the slices of reconstructed volume for the representation of the state of dispersion of the filler. Different clusters can be distinguished by having different colors from their neighbours.

We analyzed the filler volume fraction found by SBF-SEM in a 91 μm^3 volume (Fig. 4B and E). They were 6 ± 2% and 6 ± 0.4% for unmodified SiO_2 and OLLA-*g*-SiO_2, respectively. The higher standard error for the volume fraction for unmodified SiO_2 indicates the uneven distribution of filler material within a polymer matrix (Fig. 4D). The number of recognized OLLA-*g*-SiO_2 particles (3181 ± 87) compared to unmodified SiO_2 particles (1865 ± 222) in the analyzed volume was much higher (~70%) indicating better dispersion of modified silica. As the volume fractions are the same, this quantitatively demonstrates the suppressed microscopic aggregation and improved dispersibility of OLLA-*g*-SiO_2, which can be visually appreciated in the thinner slices of analyzed volume shown in Fig. 4C and F. Although the apparently better dispersion of modified silica does not guarantee the perfect distribution of the nanoparticles within the matrix, the observed aggregates of OLLA-*g*-SiO_2 were primarily on the nanoscale, possibly resulting from grafting to nanoparticle clusters rather than individual nanoparticles. These modified silica nanoparticle clusters were evenly distributed throughout the PLLA matrix compared to nanocomposites containing unmodified SiO_2. Inhomogeneous distribution of filler material will negatively influence the targeted material properties. Hence, we focused materials testing on OLLA-*g*-SiO_2 nanocomposites as the novel and best candidate for improved properties compared to pure PLLA and PHBV.

Barrier properties of nanocomposites

Two of the most essential properties of food packaging materials are oxygen permeability (OP) and water vapor permeability (WVP). OP can be assessed by determining the oxygen transmission rate (OTR). WVP can be calculated from measured water vapor transmission rates (WVTR). The gas transmission rates of the nanocomposites were measured and compared to pure PLLA and PHBV in Fig. 5. The OP for PLLA was found to be 18.3 cm^3 mm m^{-2} d^{-1} atm^{-1} and was reduced by ~38% to 11.4 cm^3 mm m^{-2} d^{-1} atm^{-1} after incorporation of 5 wt% of OLLA-*g*-SiO_2 nanofiller to the matrix. A similar trend was observed when incorporating filler material into PHBV, *i.e.*, the measured OP for pure matrix was found to be 5 cm^3 mm m^{-2} d^{-1} atm^{-1} and reduced by ~8% to 4.6 cm^3 mm m^{-2} d^{-1} atm^{-1}. However, the difference in OP between pure PHBV and PHBV nanocomposite was statistically insignificant. The observed trend is consistent with literature data on PLA[37–39] and PHBV[40,41] composites with silica suggesting that the reduction in OP could be attributed predominantly to the increased tortuous diffusion pathway for oxygen through the nanocomposite and increased crystallinity of the PLLA polymer matrix,[38,39] confirmed by the DSC (Table S1, ESI†). The crystalline phase of PLLA is less oxygen permeable than amorphous PLLA.

The WVP for PLLA nanocomposites slightly increased by ~15% compared to pure PLLA, from 1.06 g mm m^{-2} d^{-1} kPa^{-1} to 1.23 g mm m^{-2} d^{-1} kPa^{-1}. A similar effect was observed for PHBV,

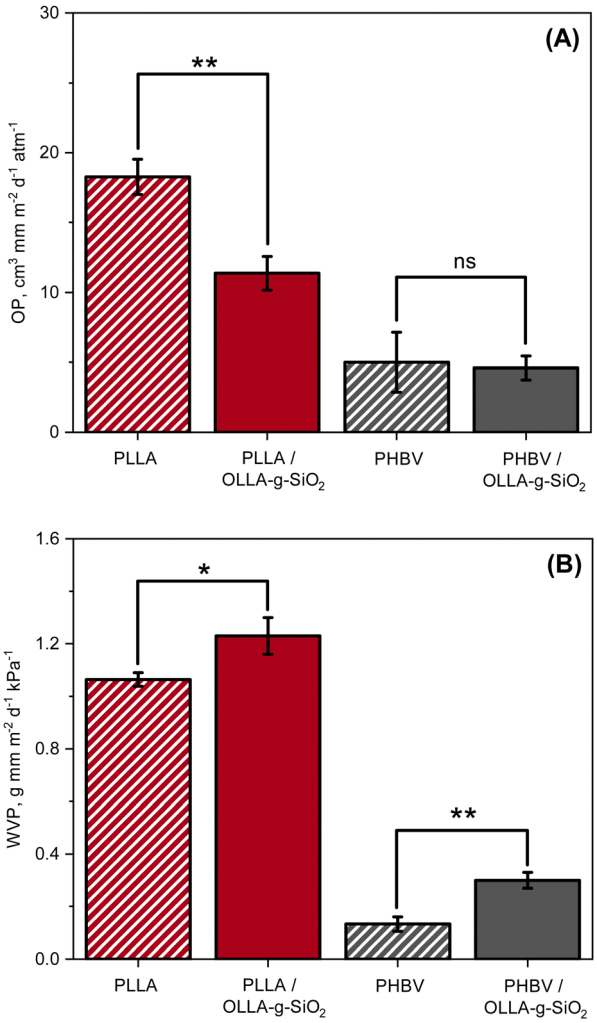

Fig. 5 Barrier properties of polymers and nanocomposites. (A) Oxygen and (B) water vapor permeability of PLLA, PLLA/OLLA-*g*-SiO_2, PHBV, and PHBV/OLLA-*g*-SiO_2.

for which WVP increased by ~124% from 0.13 g mm m^{-2} d^{-1} kPa^{-1} for pure PHVB to 0.3 g mm m^{-2} d^{-1} kPa^{-1} for PHBV/OLLA-*g*-SiO_2. These findings align with literature[42] showing that the water permeability increases because of the presence of hydrophilic SiO_2 nanoparticle cores contributing pathways for improved water transport, supported by water uptake measurements (Fig. S2, ESI†). The addition of OLLA-*g*-SiO_2 to PLLA and PHBV increased the amount of sorbed water to 1.3 ± 0.1 wt% and 0.7 ± 0.2 wt% compared to 0.8 ± 0.1 wt% and 0.5 ± 0.1 wt%, respectively. WVTR was measured in accordance to standard GB/T 1037-1988 at 38 °C, which accelerates hydrolysis of OLLA, causing structural defects in the polymer matrix and promoting water vapor penetration.[43]

Mechanical properties of nanocomposites

The effect of incorporating SiO_2 and OLLA-*g*-SiO_2 on the mechanical properties of PLLA and PHBV was investigated using tensile tests (Fig. S5, ESI†). The impact of nanofillers on the tensile modulus differed for the two polymer matrices (Table 1). The Young's modulus of both PLLA nanocomposites

Table 1 Young's modulus (E), tensile strength (σ) and elongation at break (ε) of PLLA, PLLA/SiO_2, PLLA/OLLA-*g*-SiO_2, PHBV, and PHBV/OLLA-*g*-SiO_2

Sample	E (GPa)	σ (MPa)	ε (%)
PLLA	1.7 ± 0.2	64 ± 3.7	4.6 ± 0.5
PLLA/SiO_2	1.9 ± 0.1*	67 ± 1*	5.3 ± 0.4*
PLLA/OLLA-*g*-SiO_2	1.9 ± 0.1*	62 ± 1^{ns}	10 ± 2.8***
PHBV	2.2 ± 0.1	31 ± 3.2	1.9 ± 0.2
PHBV/OLLA-*g*-SiO_2	2.1 ± 0.2^{ns}	26 ± 1.7**	2.0 ± 0.2^{ns}

Statistical significance: "***": 0–0.001, "**": 0.001–0.01, "*": 0.01–0.05, "ns": 0.05–1.0. Statistical significance was evaluated for the differences between the pure polymers (PLLA or PHBV) and their respective composites.

increased by ~12%, whereas the changes observed for the PHBV nanocomposite were insignificant. The changes in Young's moduli of the nanocomposites correlate with crystallinity of the polymer matrix (Table S1, ESI†) and are in agreement with the literature.[44,45] The tensile strength for PHBV and was reduced by ~16% after incorporation of 5 wt% of OLLA-*g*-SiO_2 into the matrix. This reduction is likely due to the remaining mismatch in interfacial properties between the filler and the polymer matrix, evidenced by the formation of agglomerates. These internal surfaces of weak adhesion led to a lower tensile strength, which correlates with the literature.[46] However, incorporating SiO_2 into PLLA resulted in ~5% increase in tensile strength, whereas the tensile strength changes for PLLA/OLLA-*g*-SiO_2 nanocomposite were statistically insignificant, being higher and dominated by the bulk material.

The elongation at break of PLLA nanocomposites increased by ~15% and ~117% for PLLA/SiO_2 and PLLA/OLLA-*g*-SiO_2, respectively, translating into an increased work of fracture of the nanocomposites and highlighting the positive effect of incorporation of (modified) silica nanoparticles. The addition of modified nano-SiO_2 resulted in an order of magnitude increase in elongation at break compared to unmodified and aggregated silica showing the benefit of well-dispersed nanoparticles within PLLA and reflecting the findings in the literature.[24] In contrast, PHBV/OLLA-*g*-SiO_2 exhibited only insignificant changes. The improvement can be attributed to the fracture energy dissipating mechanisms caused by the debonding of silica-based nanoparticles, followed by plastic void growth of polymer matrix and suppression of crack formation (Fig. S6, ESI†).[47,48] The highest elongation at break values for silica PLLA nanocomposites reported in the concentration range of filler materials we investigated is 10–37%, with higher concentrations than 5 wt% leading to no improvement.[24] The fracture energy dissipating mechanisms are strongly dependent on the homogeneity of filler network, size of the particles and their interfacial adhesion with the polymer matrix. Unmodified SiO_2 filler materials generally lead to no improvement.[24] Our results align with literature, indicating that better dispersion of the modified silica over unmodified silica results in much improved mechanical properties.

Biodegradation of nanocomposites

The biodegradation rate of nanocomposites was assessed using the modified Sturm test (Fig. S4, ESI†) and measuring the amount of CO_2 produced. The biodegradation rate of PHBV has a

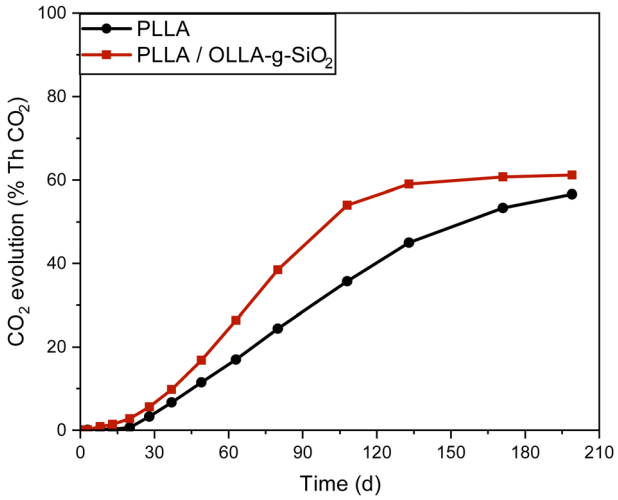

Fig. 6 CO_2 evolution of PLLA and PLLA/OLLA-*g*-SiO_2 in an aquatic test under thermophilic (58 °C) aerobic conditions because of biodegradation by a mixed bacterial inoculum deriving from biowaste compost.

predictable downward trend after the introduction of OLLA-*g*-SiO_2, which can be attributed to the lower biodegradation rate of OLLA and PLLA under thermophilic conditions compared to PHBV.[49] Therefore, the impact of nanoparticles on the biodegradability of a polymer matrix was studied only for PLLA/OLLA-*g*-SiO_2 in an aquatic setup at thermophilic conditions (Fig. 6).

PLLA nanocomposite containing OLLA-*g*-SiO_2 reached the "plateau" for CO_2 evolution faster than pure PLLA, which may be attributed to the enhanced moisture absorption leading to structural defects and improved access of hydrolases into nanocomposite due to the incorporation of SiO_2-based filler (Fig. S2, ESI†) resulting in a higher biodegradability rate of the polymer matrix.[23,50]

Conclusions

We established a scalable method to produce novel oligo-lactic acid-grafted SiO_2 nanoparticles, which has been used to produce PHBV/OLLA-*g*-SiO_2 and PLLA/OLLA-*g*-SiO_2 nanocomposites by extrusion followed by compression and injection molding. Surface modification of silica nanoparticles partially suppressed agglomerate formation and improved state of dispersion and distribution, as evidenced by a ~70% increase in the number of independent particles in the composite volume at constant volume fraction demonstrated by the 3D SBF-SEM technique.

Adding 5 wt% OLLA-*g*-SiO_2 increased the water vapor permeability of PLLA and PHBV by ~15% and ~124%, respectively, whereas the oxygen permeability of PLLA was reduced by ~38%, and for PHBV, the observed changes were insignificant. Controlling water vapor permeability is crucial to preserving perishable products and extending their shelf life, while the oxygen barrier should be improved to prevent oxidative spoilage. To make biodegradable polymers more suitable for the specific needs of the food packaging industry, it is important to develop strategies to adjust the individual gas barrier properties without compromising the mechanical performance of the material. The introduction of (modified) fillers did not significantly impact the tensile strength and resulted only in slight changes of the Young's moduli of the nanocomposites. However the elongation at break of PLLA was significantly improved by ~117% and ~15% after the addition of OLLA-*g*-SiO_2 and SiO_2, respectively, translating into an increased work of fracture and further emphasizing the significance of improving the interfacial compatibility of the nanomaterial in the polymer matrix. Incorporating OLLA-*g*-SiO_2 greatly increased the rate of hydrolytic biodegradation of PLLA nanocomposite under thermophilic conditions.

The main contribution to the improved performance of nanocomposites is attributed to the enhanced dispersibility and reduced size of OLLA-*g*-SiO_2 particles compared to SiO_2. Hence, the modification of SiO_2 nanoparticles with lactic acid oligomers and their incorporation into biodegradable materials using conventional polymer processing offers an economically feasible alternative to traditional fossil-based polymers in the food packaging industry.

Data availability

The data supporting this article have been included as part of the ESI.†

Conflicts of interest

There are no conflicts to declare.

Acknowledgements

This project has received funding from the European Union's Horizon 2020 research and innovation program under grant agreement no. 953214 (upPET). The authors thank G. Chizzola for his help with TEM imaging.

References

1 R. Geyer, J. R. Jambeck and K. L. Law, Production, use, and fate of all plastics ever made, *Sci. Adv.*, 2017, **3**, e1700782.
2 R. C. Hale and B. Song, Single-Use Plastics and COVID-19: Scientific Evidence and Environmental Regulations, *Environ. Sci. Technol.*, 2020, **54**, 7034–7036.
3 D. Knoblauch and L. Mederake, Government policies combatting plastic pollution This review comes from a themed issue on Plastic Pollution, *Curr. Opin. Toxicol.*, 2021, **28**, 87–96.
4 Proposal for a Regulation of the European Parliament and of the Council on packaging and packaging waste, amending Regulation (EU) 2019/1020 and Directive (EU) 2019/904, and repealing Directive 94/62/EC, Brussel, 2022.
5 R. Muthuraj, M. Misra and A. K. Mohanty, Biodegradable compatibilized polymer blends for packaging applications: A literature review, *J. Appl. Polym. Sci.*, 2018, **135**, 45726.

6 P. Skoczinski, M. Carus, D. De Guzman, H. Käb, R. Chinthapalli, J. Ravenstijn, W. Baltus and A. Raschka, *Bio-based Building Blocks and Polymers-Global Capacities, Production and Trends, 2020–2025*, 2021.
7 K. Madhavan Nampoothiri, N. R. Nair and R. P. John, An overview of the recent developments in polylactide (PLA) research, *Bioresour. Technol.*, 2010, **101**, 8493–8501.
8 K. W. Meereboer, M. Misra and A. K. Mohanty, Review of recent advances in the biodegradability of polyhydroxyalkanoate (PHA) bioplastics and their composites, *Green Chem.*, 2020, **22**, 5519–5558.
9 B. Laycock, P. Halley, S. Pratt, A. Werker and P. Lant, The chemomechanical properties of microbial polyhydroxyalkanoates, *Prog. Polym. Sci.*, 2013, **38**, 536–583.
10 G. Policastro, M. Fabbricino and A. Panico, Improving biological production of poly(3-hydroxybutyrate-*co*-3-hydroxyvalerate) (PHBV) co-polymer: a critical review, *Rev. Environ. Sci. Bio/Technol.*, 2021, **20**, 479–513.
11 J. W. Rhim and P. K. W. Ng, Natural biopolymer-based nanocomposite films for packaging applications, *Crit. Rev. Food Sci. Nutr.*, 2007, **47**, 411–433.
12 S. Y. Fu, X. Q. Feng, B. Lauke and Y. W. Mai, Effects of particle size, particle/matrix interface adhesion and particle loading on mechanical properties of particulate–polymer composites, *Composites, Part B*, 2008, **39**, 933–961.
13 V. D. Punetha, S. Rana, H. J. Yoo, A. Chaurasia, J. T. McLeskey, M. S. Ramasamy, N. G. Sahoo and J. W. Cho, Functionalization of carbon nanomaterials for advanced polymer nanocomposites: A comparison study between CNT and graphene, *Prog. Polym. Sci.*, 2017, **67**, 1–47.
14 L. Peponi, D. Puglia, L. Torre, L. Valentini and J. M. Kenny, Processing of nanostructured polymers and advanced polymeric based nanocomposites, *Mater. Sci. Eng., R*, 2014, **85**, 1–46.
15 S. Shi, P. Lv, C. Valenzuela, B. Li, Y. Liu, L. Wang and W. Feng, Scalable Bacterial Cellulose-Based Radiative Cooling Materials with Switchable Transparency for Thermal Management and Enhanced Solar Energy Harvesting, *Small*, 2023, **19**, 2301957.
16 Y. Chen, C. Valenzuela, X. Zhang, X. Yang, L. Wang and W. Feng, Light-driven dandelion-inspired microfliers, *Nat. Commun.*, 2023, **14**, 1–10.
17 B. Li, C. Valenzuela, Y. Liu, X. Zhang, Y. Yang, Y. Chen, L. Wang and W. Feng, Free-Standing Bacterial Cellulose-Templated Radiative Cooling Liquid Crystal Films with Self-Adaptive Solar Transmittance Modulation, *Adv. Funct. Mater.*, 2024, 2402124.
18 L. P. Singh, S. K. Bhattacharyya, R. Kumar, G. Mishra, U. Sharma, G. Singh and S. Ahalawat, Sol-Gel processing of silica nanoparticles and their applications, *Adv. Colloid Interface Sci.*, 2014, **214**, 17–37.
19 L. A. Goettler, K. Y. Lee and H. Thakkar, Layered silicate reinforced polymer nanocomposites: Development and applications, *Polym. Rev.*, 2007, **47**, 291–317.
20 Z. Pu, J. E. Mark, J. M. Jethmalani and W. T. Ford, Effects of Dispersion and Aggregation of Silica in the Reinforcement of Poly(methyl acrylate) Elastomers, *Chem. Mater.*, 1997, **9**, 2442–2447.
21 S. P. Nunes, K. V. Peinemann, K. Ohlrogge, A. Alpers, M. Keller and A. T. N. Pires, Membranes of poly(ether imide) and nanodispersed silica, *J. Membr. Sci.*, 1999, **157**, 219–226.
22 F. Wu, B. Zhang, W. Yang, Z. Liu and M. Yang, Inorganic silica functionalized with PLLA chains via grafting methods to enhance the melt strength of PLLA/silica nanocomposites, *Polymer*, 2014, **55**, 5760–5772.
23 J. Gudiño-Rivera, F. Medellín-Rodríguez, E. Ramírez-Vargas and O. Rodríguez-Fernández, Effect of grafted Mesoporous silica [SBA-15-g-OLLA] additives on the hydrolytic degradation of poly (L-lactic acid) [PLLA], *J. Polym. Res.*, 2022, **29**, 428.
24 S. Yan, J. Yin, Y. Yang, Z. Dai, J. Ma and X. Chen, Surface-grafted silica linked with L-lactic acid oligomer: A novel nanofiller to improve the performance of biodegradable poly(L-lactide), *Polymer*, 2007, **48**, 1688–1694.
25 N. Régibeau, R. G. Tilkin, C. Grandfils and B. Heinrichs, Preparation of poly-d,l-lactide based nanocomposites with polymer-grafted silica by melt blending: Study of molecular, morphological, and mechanical properties, *Polym. Compos.*, 2021, **42**, 955–972.
26 L. Wu, D. Cao, Y. Huang and B.-G. Li, Poly(L-lactic acid)/SiO2 nanocomposites via in situ melt polycondensation of L-lactic acid in the presence of acidic silica sol: Preparation and characterization, *Polymer*, 2008, **49**, 742–748.
27 Z. Feng, J. Zhong, W. Guan, R. Tian, C. Lu and C. Ding, Three-dimensional direct visualization of silica dispersion in polymer-based composites, *Analyst*, 2018, **143**, 2090–2095.
28 Y. Luan, J. Wu, M. Zhan, J. Zhang, J. Zhang and J. He, 'One pot' homogeneous synthesis of thermoplastic cellulose acetate-*graft*-poly(L-lactide) copolymers from unmodified cellulose, *Cellulose*, 2013, **20**, 327–337.
29 M. Tae Kim, Deposition behavior of hexamethydisiloxane films based on the FTIR analysis of Si–O–Si and Si–CH_3 bonds, *Thin Solid Films*, 1997, **311**, 157–163.
30 X. Wen, One-pot route to graft long-chain polymer onto silica nanoparticles and its application for high-performance poly(L-lactide) nanocomposites, *RSC Adv.*, 2019, **9**, 13908–13915.
31 E. Wojtczak, P. Kubisa and M. Bednarek, Thermal stability of polylactide with different end-groups depending on the catalyst used for the polymerization, *Polym. Degrad. Stab.*, 2018, **151**, 100–104.
32 I. A. Rahman and V. Padavettan, Synthesis of Silica Nanoparticles by Sol-Gel: Size-Dependent Properties, Surface Modification, and Applications in Silica-Polymer Nanocomposites-A Review, *J. Nanomater.*, 2012, 8.
33 H. Zou, S. Wu and J. Shen, Polymer/Silica Nanocomposites: Preparation, characterization, propertles, and applications, *Chem. Rev.*, 2008, **108**, 3893–3957.
34 D. N. Bikiaris, G. Z. Papageorgiou, E. Pavlidou, N. Vouroutzis, P. Palatzoglou and G. P. Karayannidis, Preparation by melt mixing and characterization of isotactic

polypropylene/SiO2 nanocomposites containing untreated and surface-treated nanoparticles, *J. Appl. Polym. Sci.*, 2006, **100**, 2684–2696.

35 M. Grala, Z. Bartczak and A. Różański, Morphology, thermal and mechanical properties of polypropylene/SiO2 nanocomposites obtained by reactive blending, *J. Polym. Res.*, 2016, **23**, 1–19.

36 A. Hanifpour, N. Bahri-Laleh, M. Nekoomanesh-Haghighi and M. Karimi, Synthesis and characterization of poly1-hexene/silica nanocomposites, *Polym. Test.*, 2017, **61**, 27–34.

37 X. Wen, K. Zhang, Y. Wang, L. Han, C. Han, H. Zhang, S. Chen and L. Dong, Study of the thermal stabilization mechanism of biodegradable poly(L-lactide)/silica nanocomposites, *Polym. Int.*, 2011, **60**, 202–210.

38 J. Sepulveda, C. Villegas, A. Torres, E. Vargas, F. Rodriguez, S. Baltazar, A. Prada, A. Rojas, J. Romero, S. Faba and M. J. Galotto, Effect of functionalized silica nanoparticles on the mass transfer process in active PLA nanocomposite films obtained by supercritical impregnation for sustainable food packaging, *J. Supercrit. Fluids*, 2020, **161**, 104844.

39 B. M. Pilić, T. I. Radusin, I. S. Ristić, C. Silvestre, V. L. Lazić, S. S. Baloš and D. Duraccio, Hydrophobic silica nanoparticles as reinforcing filler for poly (lactic acid) polymer matrix, *Hem. Ind.*, 2016, **7**, 73–80.

40 D. Li, J. Fu and X. Ma, Improvement in thermal, mechanical, and barrier properties of biocomposite of poly (3-hydroxybutyrate-*co*-3-hydroxyhexanoate)/modified nano-SiO2, *Polym. Compos.*, 2020, **41**, 381–390.

41 Y. Qiu, J. Fu, B. Sun and X. Ma, Sustainable nanocomposite films based on SiO2and biodegradable poly(3-hydroxybutyrate-*co*-3-hydroxyhexanoate) (PHBH) for food packaging, *E-Polymers*, 2021, **21**, 72–81.

42 Y. Bao, Y. Yang and J. Ma, Fabrication of monodisperse hollow silica spheres and effect on water vapor permeability of polyacrylate membrane, *J. Colloid Interface Sci.*, 2013, **407**, 155–163.

43 G. Schliecker, C. Schmidt, S. Fuchs and T. Kissel, Characterization of a homologous series of d,l-lactic acid oligomers; a mechanistic study on the degradation kinetics in vitro, *Biomaterials*, 2003, **24**, 3835–3844.

44 X. Wen, Y. Lin, C. Han, K. Zhang, X. Ran, Y. Li and L. Dong, Thermomechanical and optical properties of biodegradable poly(L-lactide)/silica nanocomposites by melt compounding, *J. Appl. Polym. Sci.*, 2009, **114**, 3379–3388.

45 S. Mahović Poljaček, D. Priselac, T. Tomašegović, U. S. Elesini, M. Leskovšek and M. Leskovac, Effect of the Addition of Nano-Silica and Poly(ε-caprolactone) on the Mechanical and Thermal Properties of Poly(lactic acid) Blends and Possible Application in Embossing Process, *Polymers*, 2022, **14**, 4861.

46 D. Hammiche, A. Boukerrou, Y. Grohens, N. Guermazi and F. E. Arrakhiz, Mechanical properties and biodegradation of biocomposites based on poly (hydroxybutyrate-*co*-valerate) and alfa fibers, *J. Polym. Res.*, 2020, **27**, 1–10.

47 B. Wang, X. Zhang, L. Zhang, Y. Feng, C. Liu and C. Shen, Simultaneously reinforcing and toughening poly(lactic acid) by incorporating reactive melt-functionalized silica nanoparticles, *J. Appl. Polym. Sci.*, 2020, **137**, 48834.

48 C. M. Manjunatha, A. C. Taylor, A. J. Kinloch and S. Sprenger, The cyclic-fatigue behaviour of an epoxy polymer modified with micron-rubber and nano-silica particles, *J. Mater. Sci.*, 2009, **44**, 4487–4490.

49 S. Luo and A. N. Netravali, A study of physical and mechanical properties of poly(hydroxybutyrate-*co*-hydroxyvalerate) during composting, *Polym. Degrad. Stab.*, 2003, **80**, 59–66.

50 X. Liu, Y. Zou, G. Cao and D. Luo, The preparation and properties of biodegradable polyesteramide composites reinforced with nano-CaCO3 and nano-SiO2, *Mater. Lett.*, 2007, **61**, 4216–4221.